Visible-light-driven photocatalytic N$_2$ fixation to nitrates by 2D/2D ultrathin BiVO$_4$ nanosheet/rGO nanocomposites

Shuai Shao,[a] Jun Zhang,[*a] Yuanhang Qin,[a] Likun Li,[b] Zhao-Qing Liu,[*c] Tielin Wang[*a]

[a] *Key Laboratory of Green Chemical Process of Ministry of Education, Hubei Key Laboratory of Novel Reactor and Green Chemical Technology, School of Chemical Engineering and Pharmacy, Wuhan Institute of Technology, Wuhan 430205, P. R. China*

[b] *China-Ukraine Institute of Welding Guangdong Academy of Sciences, Guangdong Provincial Key Laboratory of Advanced Welding Technology, Guangzhou, 510651, P. R. China*

[c] *School of Chemistry and Chemical Engineering/Guangzhou Key Laboratory of Clean Energy and Materials, Guangzhou University, Guangzhou 510006, China.*

[*]Corresponding author.

E-mail address: junzhang@wit.edu.cn (J. Zhang); witwangtl@hotmail.com (T. L. Wang); lzqgzu@gzhu.edu.cn (Z. Q. Liu)

Experimental details

Sample preparation

All chemicals are of analytical grade and used without further purification. Distilled water was used in all experiments. Graphene oxide (GO) was prepared from graphite by a modified Hummer's method. A solvethermal procedure was performed to prepare the 2D/2D rGO/BiVO$_4$ nanocomposite samples. In a typical synthesis, 7 mmol of BiCl$_3$, 2.88 mmol cetyltrimethyl ammonium bromide (CTAB) and appropriate amount of GO were dissolved in 60 mL of ethylene glycol (EG), the emulsion was obtained with stirring more than 40 min. After that 7 mmol of Na$_3$VO$_4$ was slowly added under drastic stirring for another 60 min. Then the yellow mixture was transferred into a 100 mL Teflon-lined autoclave, sealed and heated at 160 °C for 3 hours. The product was cooled to room temperature naturally and then washed with water and ethanol for several times, then air dried at 80 °C for 12 hours. The nominal weight contents of GO in the composites were 0.5, 1 and 5 %, and the corresponding samples were labelled as BG-0.5, BG-1 and BG-5, respectively. Moreover, the pristine BiVO$_4$ specimens were also prepared under the same experimental conditions without GO and labelled as BVO (with CTAB) and n-BVO (without CTAB).

Characterization

The crystalline phases of the obtained samples were recorded on X-ray diffraction (XRD) by an X-ray diffractometer (Rigaku, Japan) using Cu K$_\alpha$ radiation ($\lambda = 0.15418$ nm) at a scan rate (2θ) of 0.05º s^{-1}. The morphology of the samples was characterized by field emission scanning electron microscopy (FESEM) on JSM-7500 electron microscope (JEOL, Japan) operating at an accelerating voltage of 15 kV. Morphological observation was further visualized by the transmission electron microscopy (TEM) on a Tecnai G^2 F20 S-TWIN microscope with a field emission gun at a 200 kV accelerating voltage. UV-vis diffuse reflectance spectra were investigated by a UV-vis spectrophotometer (UV-2600, Shimadzu, Japan) using BaSO$_4$ powder as a reference standard. The Brunauer-Emmett-Teller (BET) surface area was carried by Micromeritics ASAP 2020 nitrogen adsorption apparatus (USA). All the samples were degassed at 150

°C before nitrogen adsorption measurements. The BET specific surface area was tested by a multipoint BET method using the adsorption data in the relative pressure (P/P_0) range of 0.05-0.25. The pore size distributions were measured utilizing desorption data by the Barrett-Joyner-Halenda (BJH) method. The pore volume and average pore size was determined by the nitrogen adsorption volume at the relative pressure (P/P_0) of 0.972. X-ray photoelectron spectroscopy (XPS) measurements were operated by an ultra-high-vacuum VG channel detector. The spectra were excited using Al K$_\alpha$ (1486.7 eV) radiation (operated at 300 W) of a twin anode in the constant analyzer energy mode with an energy of 30 eV. Time-resolved fluorescence emission spectra were surveyed by a FLS920 fluorescence lifetime spectrophotometer (Edinburgh Instruments, UK) with the excitation of 375 nm and the detection wavelength of 540 nm using silica gel as the reference standard. Surface photovoltage (SPV) spectra were measured by a surface photovoltage spectroscopy (PL-SPS/IPCE 1000 Beijing Perfect Light Technology Co., Ltd).

Photoconversion of N_2 into nitrate

A 100 mL quartz three-necked flask was used as the photoreactor for photocatalytic reaction at ambient temperature and atmospheric pressure. Before the measurement, the catalysts were washed by ultrapure water in order to avoid the disturbing of other ions. After that 0.1 g of catalysts were dispersed in 60 mL ultrapure water by ultrasonic treatment. In the experiment process, a mixture of ultrapure N_2 (99.999%) and ultrapure O_2 (99.995%) (3:1/v:v) was purged into the solution for 30 min in the dark. A 300 W Xe arc lamp through a UV-cutoff filter ($\leq$ 420 nm) was used as visible-light source. The concentration of NO_3^- and NO_2^- were tested after 3 h irradiation using an ion chromatograph (IC1010, Techcomp). The concentration of NO_2^- was found to be negligible, which suggested that during the photocatalytic NOR reaction, NO_3^- was the main product by oxidation of NO in the presence of O_2 and H_2O.

The apparent quantum efficiency (QE) under monochromatic light irradiation was determined using single wavelength filters with a bandwidth of ±5 nm. The details of the QE calculation are shown as follows:

QE(%)=100×(number of molecules nitrate generated×2)/number of incident photons

$$=100 \times M \times N_A \times 2/(I \times A \times t \times \lambda/hc)$$

Where M represents the amount of nitrate generation, N_A represents Avogadro's constant, I is the light intensity, A is the light incident area, t is the light incident time, λ is the light irradiation wavelength, h is the Plank constant, and c is speed of light.

Theoretical simulation

Density functional theory (DFT) calculations were conducted through the Vienna ab initio Simulation Package (VASP) with the projector augment wave method. Generalized gradient approximation of the Perdew-Burke-Ernzerhof (PBE) functional was used as the exchange-correlation functional. The cutoff energy was set as 500 eV, and structure relaxation was performed until the convergence criteria of energy and force reached 1×10^{-5} eV and 0.02 eV Å^{-1}, respectively. A vacuum layer of 15 Å was constructed to eliminate interactions between periodic structures of surface models. The van der Waals (vdW) interaction was amended by the DFT-D3 method of Grimme.

The adsorption energy (ΔE_{ads}) of N_2 adsorption on surface is defined as:

$$\Delta E_{ads} = E(*N_2) - E(*) - E(N_2)$$

Where $E(*N_2)$ and $E(*)$ are the total energy of surface systems with and without N_2 molecule, respectively, $E(N_2)$ is the energy of an isolated N_2 molecule. According to this definition, negative adsorption energy suggests that the adsorption process is exothermic and the adsorption system is thermodynamically stable. Contrarily, a positive value corresponds to an endothermic and unstable adsorption.

The Gibbs free energy was calculated as:

$$\Delta G = \Delta E + \Delta E_{ZPE} - T\Delta S$$

Where the ΔE, ΔE_{ZPE}, and ΔS are electronic energy, zero-point energy, and entropy difference between products and reactants. The zero-point energies of isolated and absorbed intermediate products were calculated from the frequency analysis. The frequencies and entropies of molecules in the gas phase were obtained from the National Institute of Standards and Technology (NIST) database.

Table S1. The corresponding physicochemical properties of prepared samples.

Samples	S_{BET} (m^2 g^{-1})	V_{pore} (m^3 g^{-1})	d_{pore} (nm)
BVO	34	0.25	26
n-BVO	9	0.11	37
BG-1	40	0.24	23

Table S2. Recent studies on N$_2$ photo-oxidation to NO$_3^-$ over different photocatalysts.

Photocatalyst	Light source	NO$_3^-$ yield activity	Apparent quantum efficiency	Ref.
P25(TiO$_2$)-carbon paper	Mercury lamp with UV light	3.51 mg m^{-2} h^{-1}	-	[1]
W$_{18}$O$_{49}$ nanowires	AM 1.5G, 100 mW/cm^2	0.54 mol g^{-1} h^{-1}	-	[2]
WO$_3$ nanosheets	300 W Xe lamp	1.92 mg g^{-1} h^{-1}	0.11% (380 nm)	[3]
Few-layer g-C$_3$N$_4$	300 W Xenon lamp	109.96 μmol L^{-1} h^{-1} g^{-1}	-	[4]
TiO$_2$/WO$_3$	Thermal-assisted photocatalysis	NO yield: 0.16 mmol g^{-1} h^{-1}	0.31% (365 nm)	[5]
BiVO$_4$/rGO	300 W Xe lamp, >420 nm	1.45 mg h^{-1} g^{-1}	0.64% (420 nm)	This work

Table S3. Time-resolved fluorescence decay data of BVO and BG-1 composite saamples.

Sample	τ_1 (ns)	A_1 (%)	τ_2 (ns)	A_2 (%)	τ_3 (ns)	A_3 (%)	τ_{ave} (ns)
BG-1	0.54	44.65	2.79	41.87	11.33	13.48	2.94
BVO	0.40	55.67	3.00	34.20	25.00	10.13	3.78

Table S4. The reaction Gibbs free energies (ΔG) of all steps for N_2 photooxidation over $BiVO_4$ and $BiVO_4$/rGO composite.

Steps	ΔG (eV) $BiVO_4$	ΔG (eV) $BiVO_4$/rGO
*H_2O	0.11	-1.38
*OH	2.17	1.34
*O	2.68	2.00
*(O+H_2O)	0.12	0.98
*(O+OH)	0.36	1.39
*(O+O)	0.98	0.55
*2NO	0.41	0.55
*+2NO	-0.07	1.32
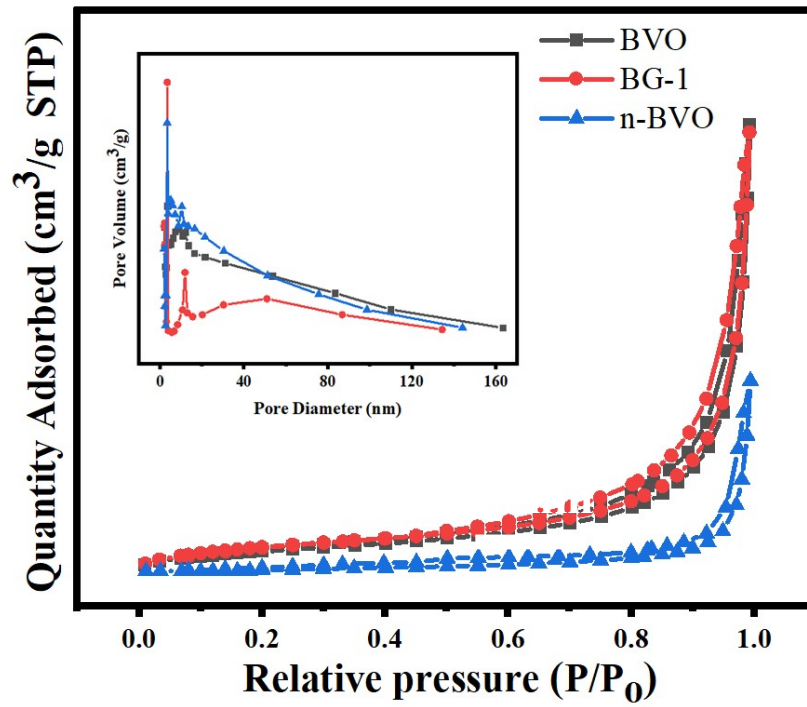
Figure S1. Nitrogen adsorption-desorption isotherms and the corresponding pore size distribution curves (inset) of BVO, n-BVO and BG-1 samples.
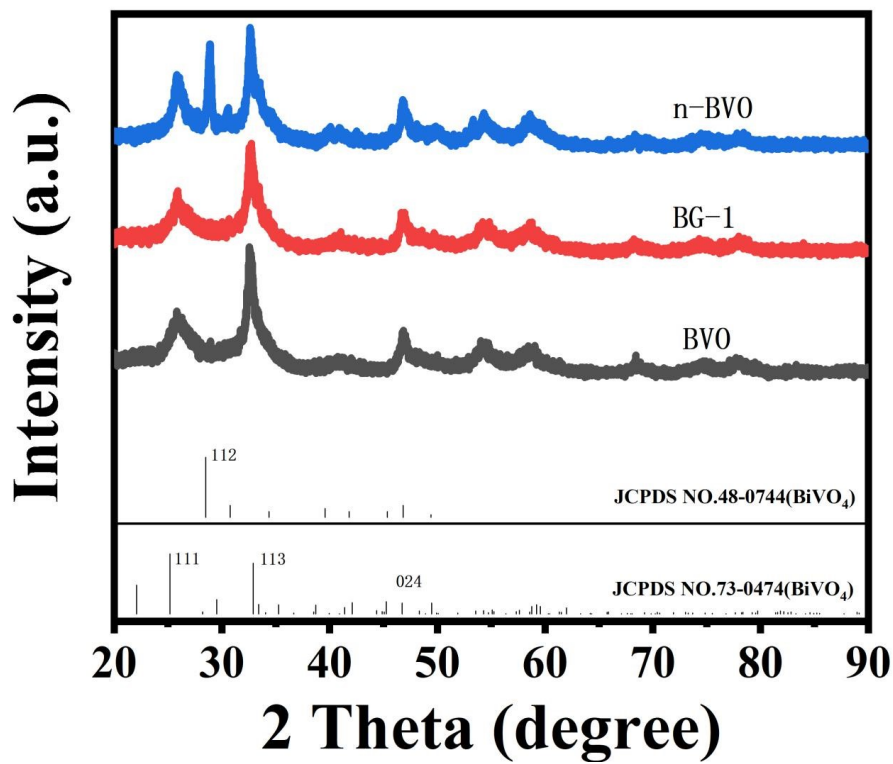
Figure S2. XRD patterns of the as-prepared samples.
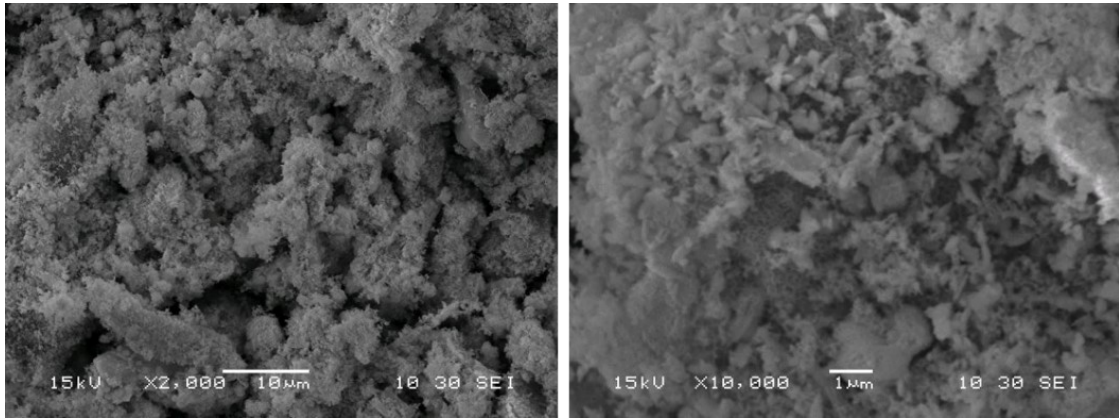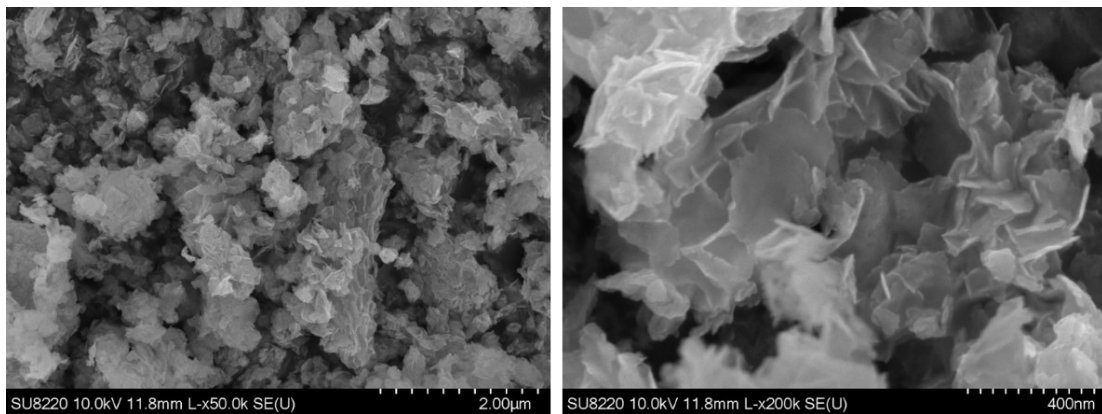
Figure S3. SEM images of n-BVO sample.

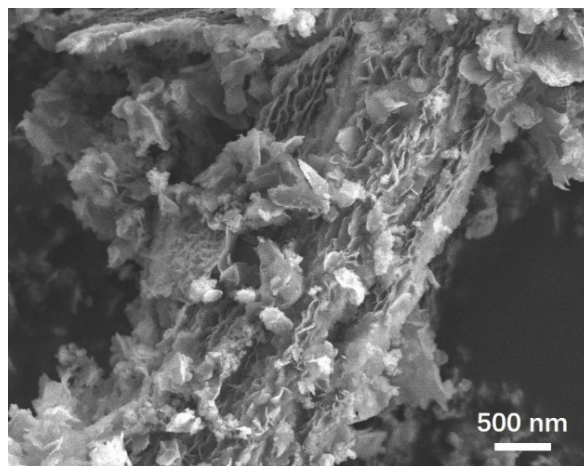**Figure S4.** SEM images of BVO sample.
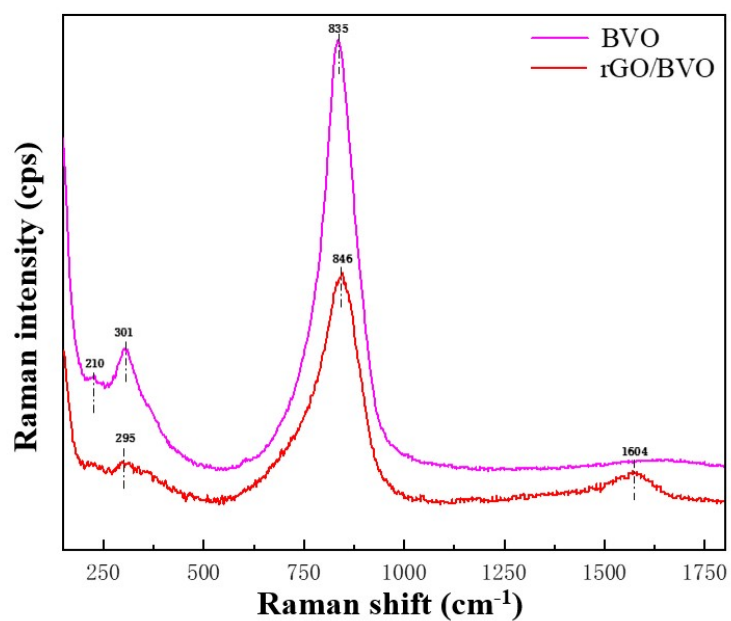

Figure S5. SEM image of BG-1 sample.
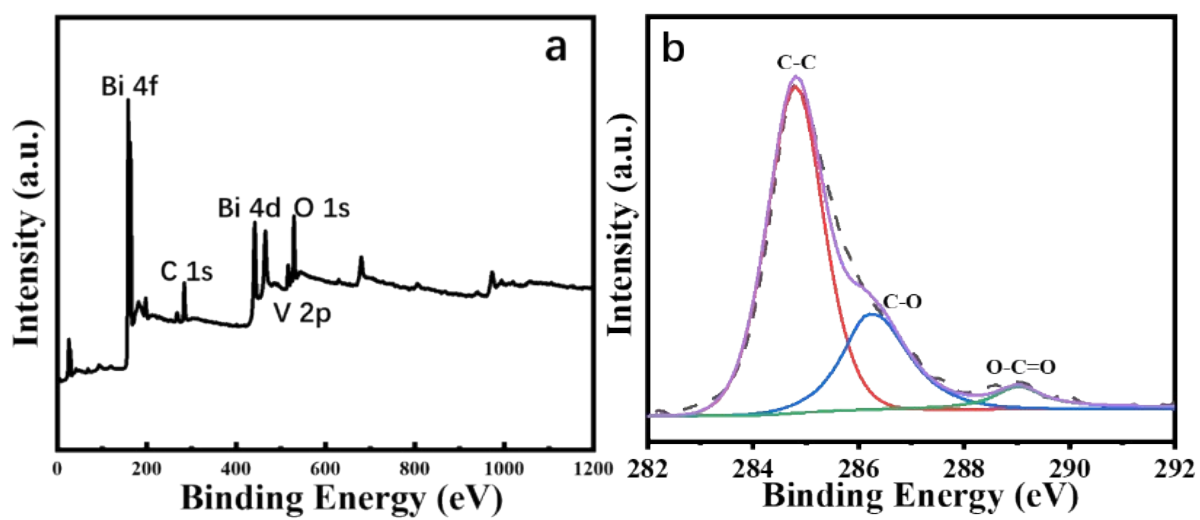
Figure S6. Raman spectra of BVO and BG-1 samples.

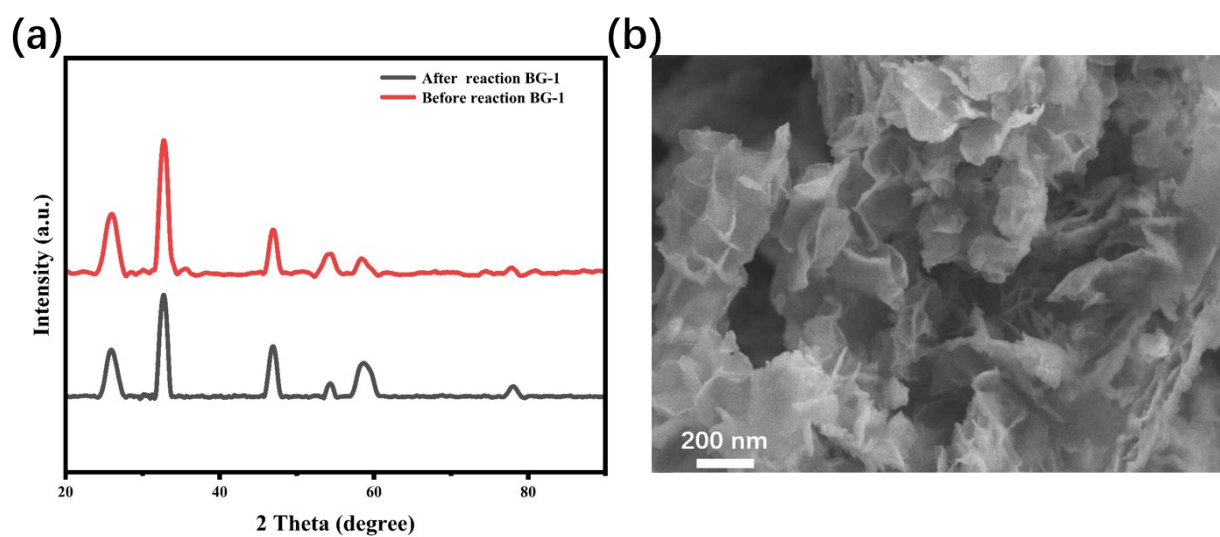**Figure S7.** (a) XPS spectrum and (b) high-resolution XPS spectra of C 1s from BG-1 sample.

Figure S8. (a) XRD patterns of BG-1 sample before and after photocatalytic reaction, (b) SEM image of BG-1 sample after photocatalytic reaction.
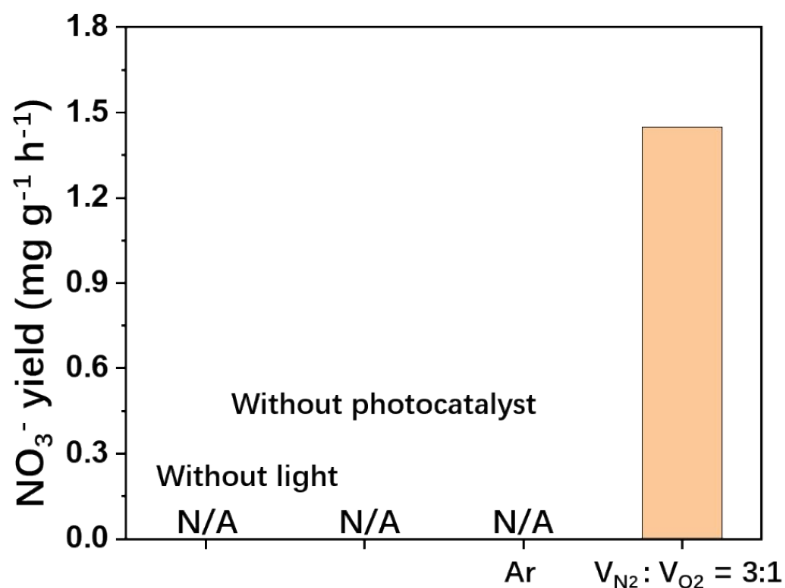
Figure S9. The control experiments that nitrate formation under different conditions on BG-1 sample. The water oxidation reaction could compete with the photocatalytic NOR. Indeed, the O_2 can be detected (13.6 μmol h^{-1}) and no NO_3^- can be detected when only pure N_2 was used as purge gas. These results clearly suggested that the water oxidation reaction could be occurred during the photocatalytic NOR reaction and O_2 indeed participated in the formation of NO_3^-.
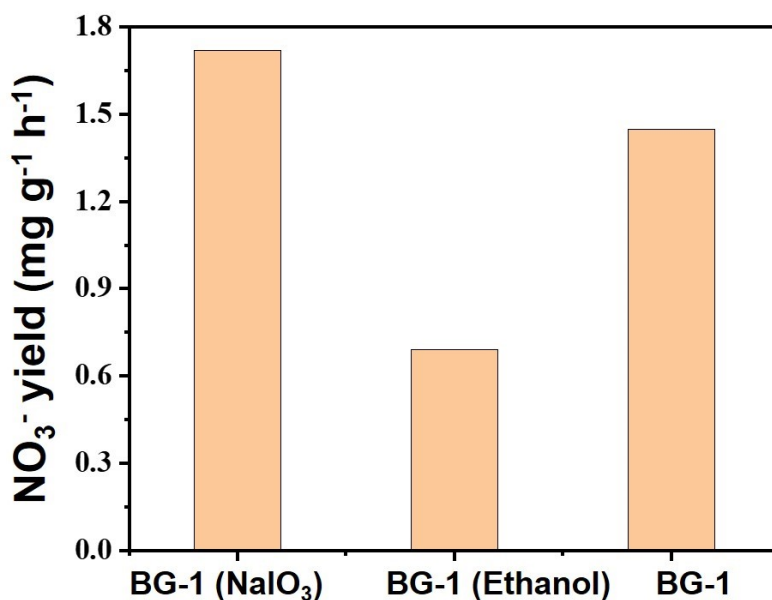

Figure S10. The control experiments that nitrate formation under different conditions on BG-1 sample.
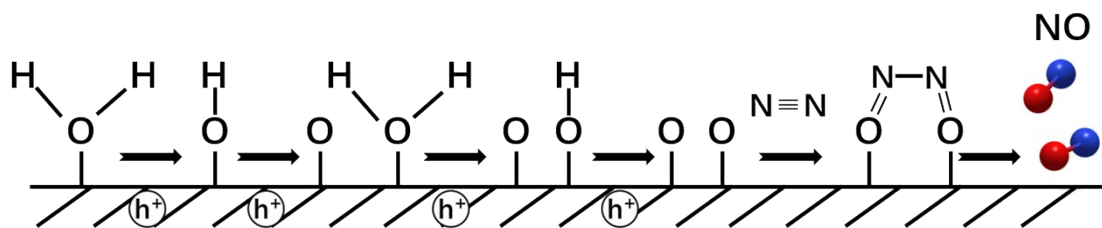
Figure S11. The proposed mechanism of N_2 photocatalytic oxidation to NO over $BiVO_4$/rGO composite.

References

[1]   S. J. Yuan, J. J. Chen, Z. Q. Lin, W. W. Li, G. P. Sheng and H. Q. Yu, *Nature Commun.*, 2013, **4**, 2249.

[2]   W. Ren, Z. Mei, S. Zheng, S. Li, Y. Zhu, J. Zheng, Y. Lin, H. Chen, M. Gu and F. Pan, *Research (Washington, D.C.)*, 2020, **2020**, 3750314-3750314.

[3]   Y. Liu, M. Cheng, Z. He, B. Gu, C. Xiao, T. Zhou, Z. Guo, J. Liu, H. He, B. Ye, B. Pan and Y. Xie, *Angew. Chem. Int. Edit.*, 2019, **58**, 731-735.

[4]   Y. Li, M. Ti, D. Zhao, Y. Zhang, L. Wu and Y. He, *J. Alloy. Compd.*, 2021, **870**, 159298.

[5]   Y. Yu, C. Wang, Y. Yu, Y. Huang, C. Liu, S. Lu and B. Zhang, *J. Mater. Chem. A*, 2020, **8**, 19623-19630.